Observations of eastward propagation of atmospheric intraseasonal oscillations from the Pacific to the Atlantic

Wei Yu,[1] Weiqing Han,[2] Eric D. Maloney,[3] David Gochis,[1] and Shang-Ping Xie[4]

Received 19 April 2010; revised 20 September 2010; accepted 29 September 2010; published 19 January 2011.

[1] Significant 40–60 day intraseasonal variability in surface winds, sea level, and thermocline depth were observed in the tropical Atlantic during the Atlantic Niño year of 2002. Satellite-derived QuikSCAT winds and NOAA Outgoing Longwave Radiation (OLR) measurements for the period of 2000–2006, together with reanalysis of winds from a longer record, are analyzed to understand the sources of this 40–60-day wind variability and the global propagation of the Madden-Julian Oscillation (MJO) surface signatures. The results demonstrate that the MJO propagated eastward from the Indo-Pacific Ocean to the Atlantic during winter and spring of 2002, causing 40–60 day wind variations in the equatorial Atlantic. The Isthmus of Panama appears to be a dominant pathway for these surface wind anomalies to propagate into the Atlantic, where they can produce important climate impacts. This result is consistent with previous work that has demonstrated a strong MJO influence on the North American Monsoon (NAM) region, and complements other work demonstrating the propagation of intraseasonal wind anomalies and accompanying sea level pressure signals associated with dry equatorial Kelvin waves that reach the Caribbean through the Panama gap. The MJO is also shown to have a large influence on the subtropical Atlantic Ocean. Seasonality of the MJO impact on Atlantic surface winds is investigated using data from an extended record, and the most direct influence is found to be during boreal winter and spring, with a delayed influence during summer and fall.

Citation: Yu, W., W. Han, E. D. Maloney, D. Gochis, and S.-P. Xie (2011), Observations of eastward propagation of atmospheric intraseasonal oscillations from the Pacific to the Atlantic, *J. Geophys. Res.*, *116*, D02101, doi:10.1029/2010JD014336.

1. Introduction

[2] The Madden-Julian Oscillation (MJO) [*Madden and Julian*, 1971] is the most prominent mode of tropical atmospheric intraseasonal variability. It is well known to have a global eastward propagating signal, with a propagation speed of approximately 5 m/s in the Indian and western Pacific Oceans. The MJO is climatically important because it can have significant impacts on the El Niño–Southern Oscillation (ENSO) [e.g., *Moore and Kleeman*, 1999; *McPhaden*, 1999; *Takayabu et al.*, 1999; *Kessler and Kleeman*, 2000], the Asian-Australian monsoon [*Sikka and Gadgil*, 1980; *Yasunari*, 1981; *Krishnamurti and Subramanyam*, 1982; *Webster*, 1983; *Wang and Xie*, 1997; *Lawrence and Webster*, 2001; *Lau and Waliser*, 2005], the Indian Ocean Dipole [e.g., *Rao and Yamagata*, 2004; *Han et al.*, 2006], and tropical cyclones [e.g., *Maloney and Shaman*, 2008].

[3] Many previous studies have revealed the global influences of the MJO. Strong MJO signals have been observed in the North American Monsoon (NAM) [e.g. *Higgins and Shi*, 2001; *Barlow and Salstein*, 2006; *Lorenz and Hartmann*, 2006], where positive zonal wind anomalies in the eastern tropical Pacific are followed by anomalous precipitation in Mexico and the southwest United States several days later. *Foltz and McPhaden* [2004] showed that intraseasonal surface wind variability is prominent in the subtropical and midlatitude Atlantic Ocean, where surface winds are significantly correlated with MJO signals in the Indo-Pacific Ocean. *Jones and Schemm* [2000] demonstrated that the South Atlantic Convergence Zone (SACZ) exhibits a wide range of intraseasonal variability, and that 30–70 day variations are directly related to the MJO. *Maloney and Hartmann* [2000] showed that the MJO can affect the Atlantic, and demonstrated a link between the MJO and hurricane activity in the Gulf of Mexico and the Caribbean Sea. Given that the cold sea surface temperatures (SSTs) in the eastern Pacific cold tongue region inhibit convection,

[1]Research Applications Laboratory, National Center for Atmospheric Research, Boulder, Colorado, USA.
[2]Department of Atmospheric and Oceanic Sciences, University of Colorado, Boulder, Colorado, USA.
[3]Department of Atmospheric Science, Colorado State University, Fort Collins, Colorado, USA.
[4]International Pacific Research Center, University of Hawaii, Honolulu, Hawaii, USA.

Copyright 2011 by the American Geophysical Union.
0148-0227/11/2010JD014336

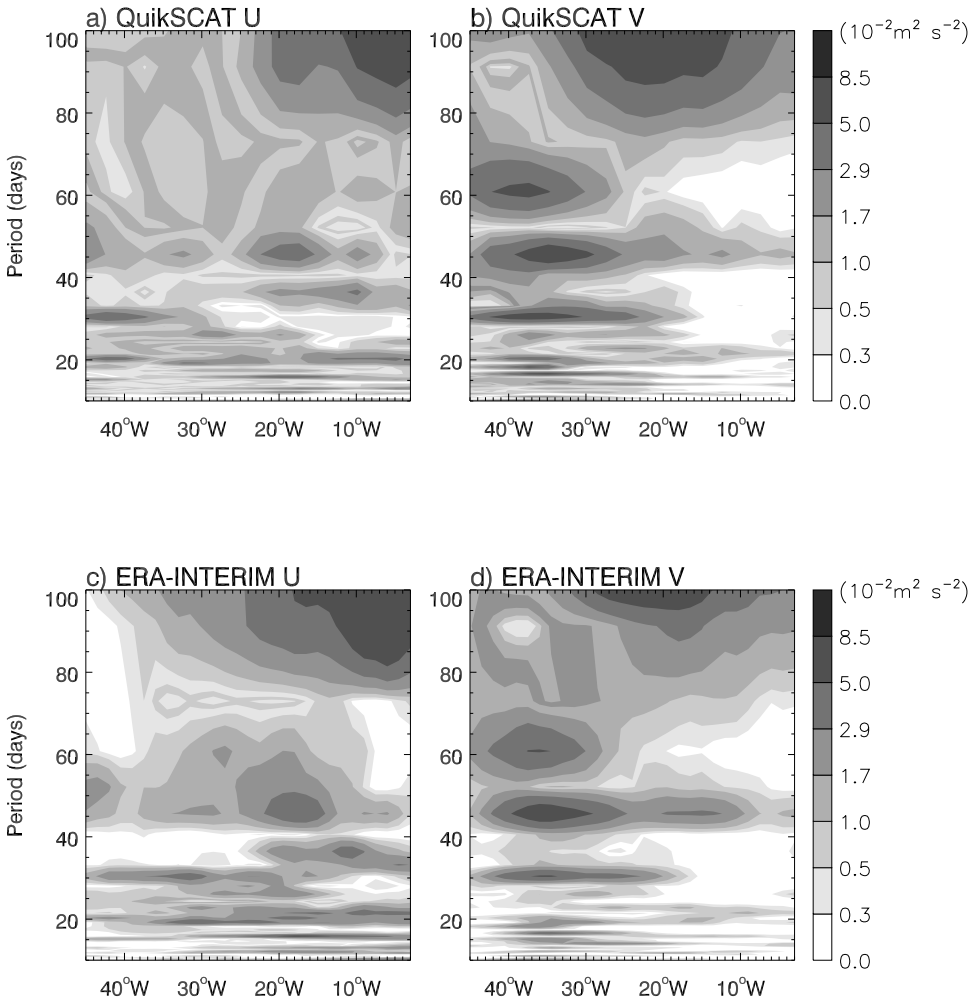

Figure 1. Variance spectra of surface wind (10 m) along the Atlantic equator (5°S–5°N averaged) based on daily winds of 2002. (a) QuikSCAT zonal wind; (b) QuikSCAT meridional wind; (c) ERA-Interim zonal wind; and (d) ERA-Interim meridional wind.

the South American continent blocks continuous air-sea interaction, and the Andes block eastward propagation, the actual mechanisms by which the MJO influences the tropical Atlantic and the propagation of the MJO surface signatures into that basin are still not well characterized.

[4] Interestingly, in the equatorial Atlantic Ocean, satellite and in situ observations show significant spectral peaks at 40–60 day periods in surface winds, sea level, and thermocline depth [*Han et al.*, 2008]. Results from numerical model experiments demonstrate that this sea level and thermocline depth variability results mainly from the first and second baroclinic modes of oceanic equatorial Kelvin waves forced by 40–60 day equatorial zonal wind anomalies. The significant 40–60 day peaks in zonal and meridional winds, which appeared in both the Quick Scatterometer (QuikSCAT) and Pilot Research Moored Array in the Tropical Atlantic (PIRATA) data, were found to be especially strong in 2002, a year when anomalously warm temperatures or a so-called "Atlantic Niño" event occurred [*Fu et al.*, 2007]. *Han et al.* [2008] also found that 40–60 day zonal wind anomalies in the central-western equatorial Atlantic basin for the 2000–2006 period were significantly correlated with sea level anomalies across the equatorial Atlantic basin, with simultaneous and lag correlation values ranging from 0.62 to 0.74 ($p \leq 0.05$). *Han et al.* [2008], however, did not explain the origin of the strong 40–60 day wind anomalies.

[5] *Matthews* [2000] suggested that sea level pressure anomalies associated with a global dry equatorial Kelvin wave that travel at a speed of approximately 35 m/s can propagate into the Atlantic through the gap at Panama. Such intraseasonal Kelvin waves can be excited by MJO heating in the Eastern Hemisphere [*Matthews*, 2000; *Small et al.*, 2010]. Our study builds on this previous work. We will address the extent to which the MJO plays an important role in causing strong 40–60 day timescale surface wind anomalies in the equatorial Atlantic. This will be first done during 2002, and then, using a longer record, explore the seasonality and propagation pathways by which surface wind and convection associated with the MJO affect the Atlantic Ocean.

2. Data and Method

[6] MJO propagation can be effectively diagnosed using Outgoing Longwave Radiation (OLR) and winds [*Arkin and*

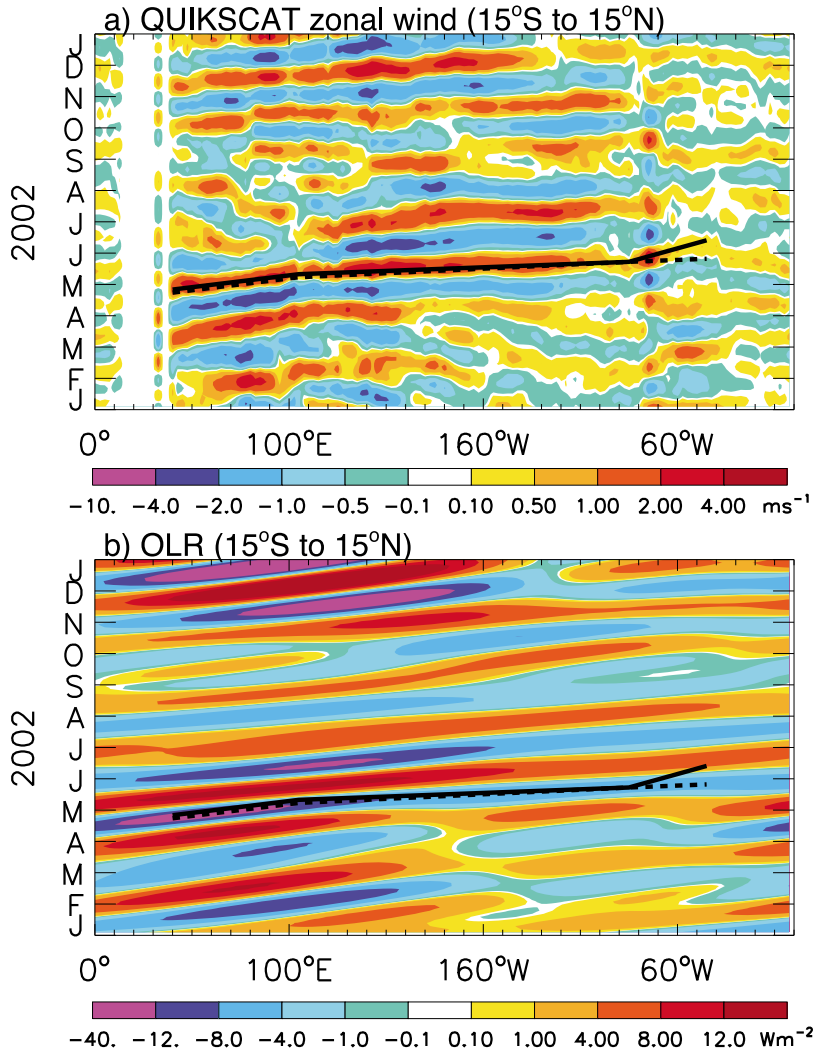

Figure 2. (a) Longitude-time diagram of 30–70 day band-pass filtered QuikSCAT 10 m zonal wind averaged from 15°S to 15°N during 2002; (b) same as Figure 2a, but for 30–70 day OLR data which have been restrictively filtered to eastward wave numbers 1–3. Two black phase curves are QuikSCAT (solid curve) and OLR (dashed curve).

Ardanuy, 1989; *Liebmann and Smith*, 1996; *Jones et al.*, 2004; *Matthews*, 2000]. Hence, 3 day mean QuikSCAT ocean surface wind vectors and NOAA interpolated OLR data from 2000 to 2006 are used to diagnose intraseasonal variability using 30–70 day band-pass filtered fields [*Duchon*, 1979]. To minimize the influence of missing values due to incomplete sampling and rain contamination, we averaged the 0.25° × 0.25° resolution QuikSCAT winds onto 2.5° × 2.5° grids. To support inferences on convective activity provided by the OLR in both the tropical and subtropical oceans, we also analyzed the 1° × 1° Global Precipitation Climatology Project (GPCP) precipitation data, the 2.5° × 2.5° Climate Prediction Center (CPC) merged analysis of precipitation (CMAP) product, and 0.7° × 0.7° European Center for Medium-Range Weather Forecasts (ECMWF) Reanalysis (ERA) Interim precipitation data [*Simmons et al.*, 2007; *Allan et al.*, 2010; *Xie and Arkin*, 1997].

[7] To isolate the MJO signals, OLR data were filtered to 30–70 day periods and eastward wave numbers 1–3, consistent with previous studies [*Hendon and Salby*, 1994; *Jones and Schemm*, 2000; *Foltz and McPhaden*, 2004]. A broad 20–100 day filter with eastward wave numbers 1–6, following the suggestion of the U. S. Climate Variability and Predictability Research Program (CLIVAR) MJO working group [*CLIVAR MJO Working Group*, 2009] and *Wheeler and Kiladis* [1999], is also applied to compare with the extracted 30–70 day MJO signals to ensure that the signals examined here are not an artifact of the narrow response function used. Intraseasonal variance, spectral coherence analysis, and correlation analysis were performed using QuikSCAT winds to demonstrate the effects of the MJO on surface winds in the tropical Atlantic Ocean. Surface winds from ERA-Interim data with 1.5° resolution from 1990 to 2007 and the 40 year reanalysis (ERA40) with 2.5° resolution for 1960–2001 were also analyzed in

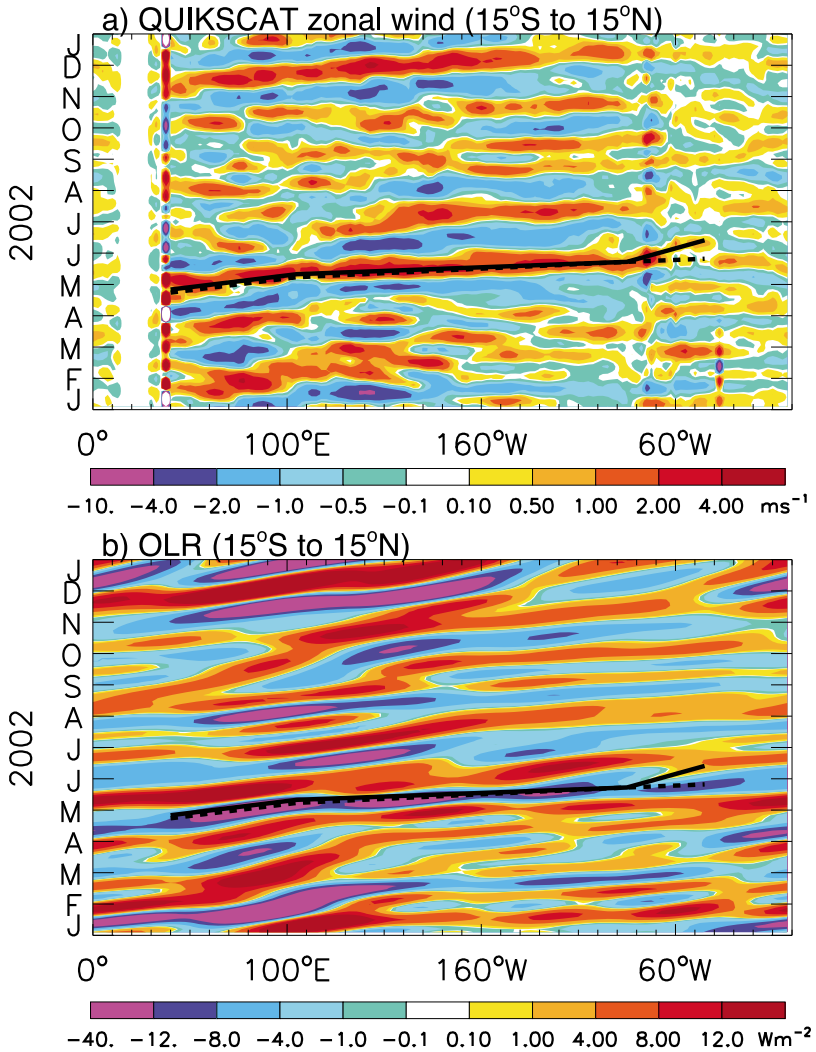

Figure 3. Same as Figure 2, except for 20–100 day band-pass filter, in which OLR data has been restrictively filtered to eastward wave numbers 1–6.

order to assess the robustness of the results for longer periods. Because QuikSCAT winds are not retrieved over land, we cannot use the spatial filter to extract the MJO signals for QuikSCAT, and thus only filter QuikSCAT winds to 30–70 days.

3. Results

3.1. Observed Intraseasonal Variability in the Tropical Atlantic

[8] Figures 1a–1d show Atlantic variance spectra of surface winds along the equator during 2002 from QuikSCAT and ERA-Interim data. Both zonal and meridional winds exhibit strong spectral peaks at intraseasonal periods, among which 40–60 day peaks are evident across most of the equatorial basin in both QuikSCAT and ERA-Interim data, consistent with *Han et al.* [2008]. Strong spectral power occurs at periods greater than 80 days in the eastern and central Atlantic basin, which is associated with the strong seasonal (annual and semiannual) cycle.

3.2. Evidence of MJO Propagation into the Atlantic During 2002

[9] Figure 2 shows longitude-time diagrams of the 30–70 day band-pass filtered QuikSCAT surface zonal wind and OLR anomalies averaged from 15°S to 15°N during 2002. Note that the OLR field is further band-pass filtered to zonal wave numbers 1–3. The large-scale features and eastward propagation of the 30–70 day wind anomalies (Figure 2a) agree well with the MJO signals in OLR (Figure 2b) in terms of a consistent phase relationship and amplitude, suggesting that the 30–70 day QuikSCAT wind anomalies are largely associated with the MJO. During January–July, the maximum 30–70 day wind anomalies are observed in the Indian and western Pacific oceans, and subsequently propagate into the Atlantic Ocean, although the Atlantic manifestation of the wind anomalies is weaker relative to the Indo-Pacific sector. Eastward propagating MJO events occur with gradually increasing strength during boreal winter and spring of 2002, reaching a maximum in May and then becoming weaker during summer. To ensure that the narrow filtering we use does not too strongly constrain our

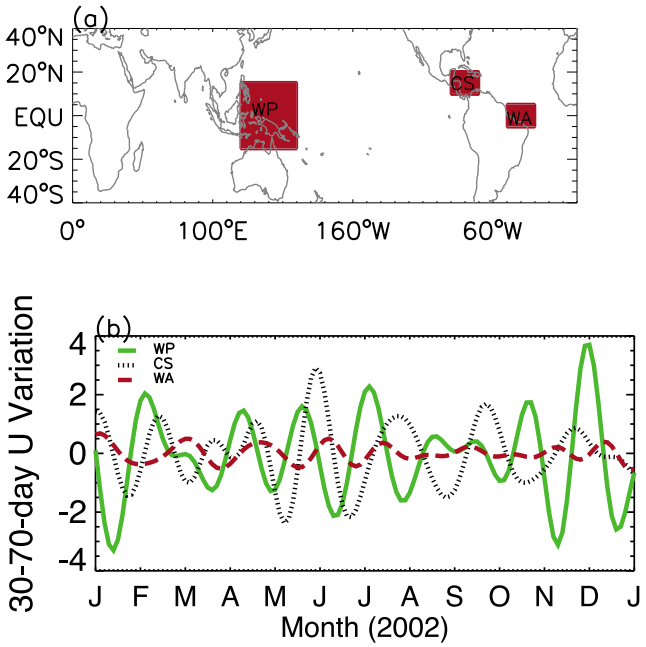

Figure 4. The time series of domain-averaged 30–70 day zonal wind variations from QuikSCAT. WP, 15°S–15°N and 120°E–160°E; CS, 10°S–20°N and 90°W–70°W; WA, 5°S–5°N and 50°W–30°W.

results, we also applied a wider 20–100 day filter as a sensitivity test. Results are similar to those derived using a narrower filter, as shown in both QuikSCAT zonal wind and OLR anomalies, except that signals are higher amplitude and noisier (Figure 3). MJO propagation from the Indian Ocean to the Atlantic is very clear during April and May in both Figure 2 and Figure 3, with propagation speeds of approximately 4.7 m/s from the Indian Ocean to the western Pacific and 14.5 m/s from the central Pacific to the Atlantic, as indicated by their phase lines. These values generally agree with the well-documented MJO propagation speed of ~5 m/s in convective regions across the Indian and western Pacific oceans, and 10–15 m/s in the Western Hemisphere [e.g., *Hendon and Salby*, 1994]. The basic propagation patterns are consistent for both OLR and winds, with winds slightly lagging enhanced convection.

[10] In contrast, during boreal summer and fall of 2002, convection associated with the MJO is weaker in the western Atlantic Ocean compared to winter and spring. In the eastern equatorial Atlantic basin (20°W to 0°E), however, impacts of the westward propagating signals are observed during May–September (Figure 2a). The westward propagation of intraseasonal anomalies across the African monsoon region into the Atlantic has been addressed in previous studies [e.g., *Matthews*, 2004; *Janicot et al.*, 2009]. In this paper, we focus on examining eastward propagating MJO influences.

[11] QuikSCAT winds cannot be retrieved over the South American continent. The continuous eastward propagation of 30–70 day wind anomalies in Figures 2a and 3a across 70°W is derived from comparatively fewer sampling points in the Caribbean Sea to the north of Colombia and Venezuela and near the Isthmus of Panama. This suggests that the MJO propagating signal is present in the surface winds near the Isthmus of Panama. An examination of ERA-Interim surface winds over the South American continent averaged from 10°S to 10°N does not indicate eastward propagation within this equatorial band (figure not shown), indicating that MJO signals in surface winds may propagate into the Atlantic primarily through the Panama area. This point will be further demonstrated below.

[12] Figure 4 shows the time series of 30–70 day filtered surface zonal wind anomalies during 2002 averaged over three regions; 15°S–15°N and 120°E–160°E in the western Pacific (WP), 10°N–20°N and 90°W–70°W in the Caribbean Sea (CS), and 5°S–5°N and 50°W–30°W in the western equatorial Atlantic (WA). In the WP region, westerly wind anomalies associated with the MJO obtain large amplitudes [e.g., *McPhaden*, 1999]. The choice of the CS region is based on the propagation signal diagnosed in Figures 2 and 3, which suggests that the MJO enters the Atlantic through the Isthmus of Panama and the CS. The WA region is chosen based on the observed 40–60 day zonal wind variability documented by *Han et al.* [2008] and shown in Figure 1. The phase lags from the WP to the CS and subsequently to the WA exhibit relatively consistent behavior from January to July. These lags indicate eastward propagation of the westerly wind anomalies from the WP to the WA through the CS, consistent with Figure 2. Note that Figure 2 is based on 15°S–15°N average, whereas Figure 4b is based on the three key regions shown in Figure 4a. Therefore, the two analyses may not be always consistent. From July to December, the clean phase progression differs from that in January–July, indicating that the MJO influence during boreal summer and fall is more complex. As mentioned above, in addition to the eastward pathway, the MJO can affect equatorial Atlantic winds by exciting westward propagating Rossby waves [*Matthews*, 2004] from the Indian Ocean during summer and fall. *Thorncroft et al.* [2003] and *Sultan and Janicot* [2003a, 2003b] suggest that winds associated with the West African monsoon, which have biweekly and 25–60 day dominant periods, can significantly affect the tropical Atlantic Ocean through westward propagation.

3.3. Evolution of the MJO During 2002

[13] Figure 5a shows the time evolution of the 30–70 day filtered QuikSCAT wind and OLR anomalies during May 2002 associated with the strong MJO event that propagated into the Atlantic (see Figure 2). On May 1, in the tropical Indian Ocean, strong convection (large amplitude negative OLR anomaly) is symmetric about the equator. Associated with the convection, a westerly wind anomaly prevails in the central and western Indian Ocean. In subsequent days, the convective maximum accompanied by the westerly wind anomaly, moves into the central-western Pacific (e.g., May 13). Meanwhile, an off-equatorial convective maximum north of the equator in the central Pacific (near 160°W, 20°N) also moves eastward. By May 25, the strong convection and its associated westerly wind anomaly propagate into the NAM region and the Caribbean Sea. Hurricane Alma, formed in the east Pacific during this period, was coincident with this MJO event. The evolution of tropical and subtropical convective activity shown by the OLR data above is further confirmed by using 30–70 day GPCP pre-

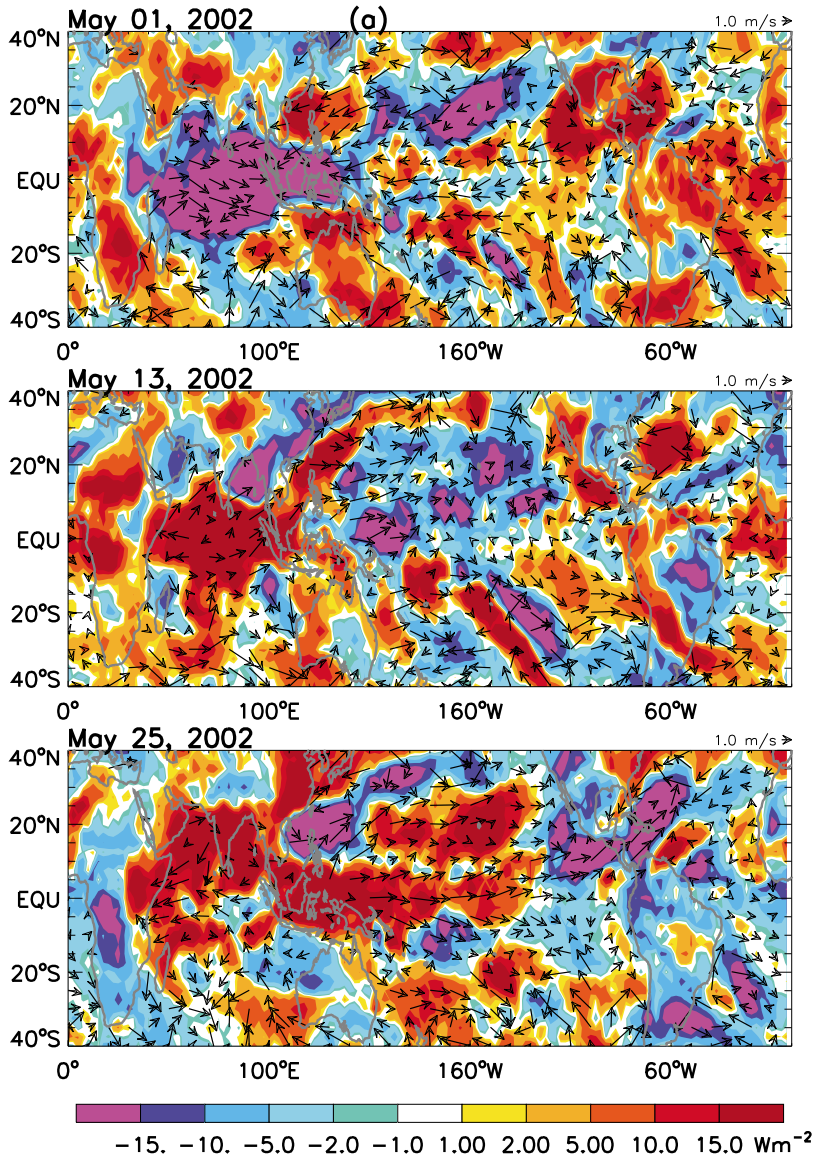

Figure 5. (a) The 30–70 day band-pass filtered OLR (color contours) and QuikSCAT winds (arrows); (b) the 30–70 day band-pass filtered GPCP precipitation (color contours) and ERA-Interim winds (arrows); (c) the 30–70 day band-pass filtered OLR (color contours) and 850 mbar ERA-Interim winds (arrows) with eastward wave numbers 1–3.

cipitation anomalies with 1° × 1° resolution (Figure 5b). Consistent precipitation patterns are also obtained using 30–70 day, 2.5° × 2.5° CMAP and 0.7° × 0.7° ERA-Interim precipitation data (figures not shown). This signal is consistent with the work of *Martin* [2010], who showed using GPCP precipitation during 1997–2008 that intraseasonal precipitation variability in the Caribbean Sea is associated with variations in the Caribbean Low Level Jet, which is modulated by the MJO.

[14] To understand the role played by the MJO, 30–70 day band-pass filtered OLR and 850 mbar wind anomalies from ERA-Interim data are further band-pass filtered to eastward zonal wave numbers 1–3 (Figure 5c). Anomalous 30–70 day convection and westerly surface winds shown in Figure 5a are associated with the strong May 2002 MJO event (see Figures 5c, 2b, and 3b). This event was also prominent in the multivariate MJO index of *Wheeler and Hendon* [2004, Figures 5 and 12]. On May 1, maximum convection together with westerly wind anomalies appears in the central and eastern equatorial Indian Ocean (Figures 5a–5c, top panels), where anomalous convergence occurs at 850 mbar and divergence occurs at 200 mbar (not shown), consistent with the baroclinic structure of the MJO described by *Jones and Carvalho* [2006] and *Hendon and Salby* [1994]. In the western equatorial Indian Ocean (50°E), cyclonic surface wind circulations exist (centered near 50°E, 25°S and 60°E, 25°N), consistent with the Gill model of a Rossby wave response to the enhanced diabatic heating. East of the equatorial convective maximum, a tongue of negative equatorial OLR anomalies together with easterly wind and convergence

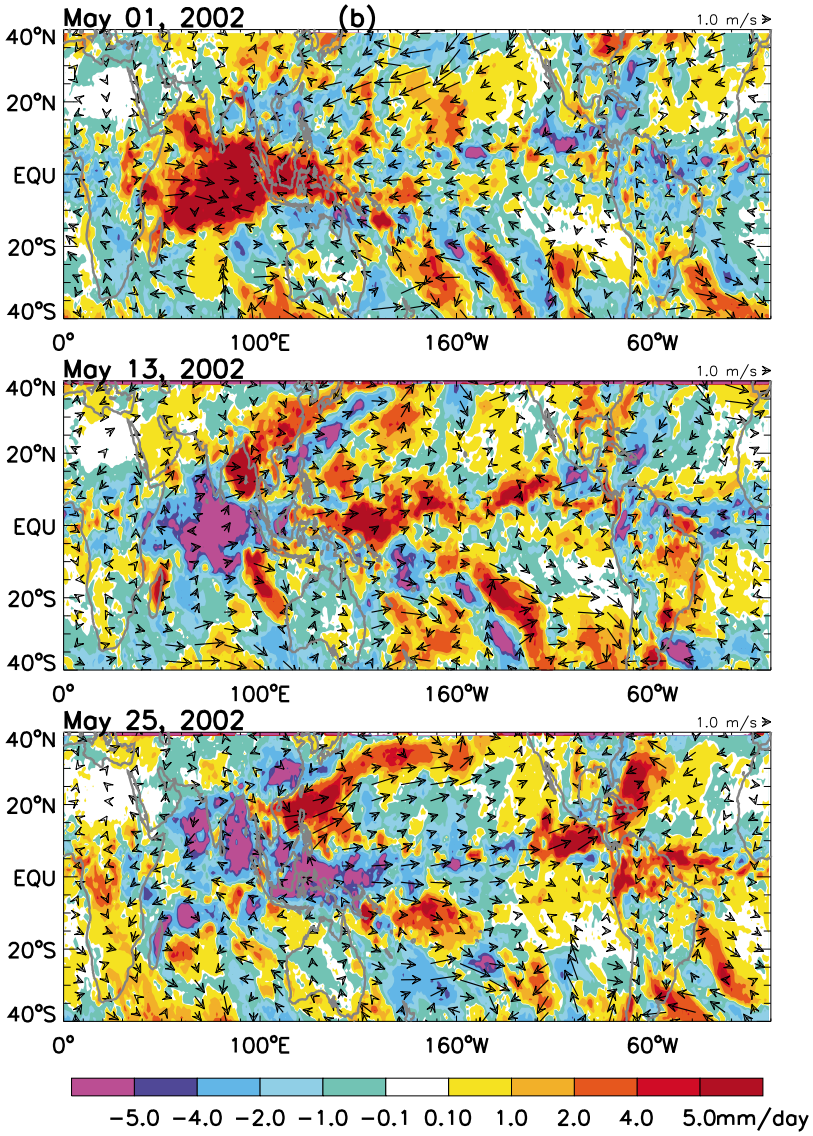

Figure 5. (continued)

anomalies that resemble a Kelvin wave extends eastward to the western Pacific. This scenario agrees well with the coupled Kelvin-Rossby wave packet structure associated with the MJO [e.g., *Wang and Xie*, 1997]. The dominance of wave number 1 on the equator and wave number 2 off the equator on May 1 (shown in Figure 5c) is also consistent with MJO structure [*Hendon and Salby*, 1994].

[15] On May 13, the coupled Kelvin-Rossby wave packet discussed above propagates eastward into the western Pacific (Figure 5c, middle panel). By May 25 the convection anomaly along the equator is significantly weakened east of the dateline and the disturbance propagates at a much faster speed into the Atlantic (Figure 5c, bottom panel). This scenario is consistent with the global behavior of the MJO as seen in work by *Matthews* [2000] and other authors. Near the dateline, the fast equatorial Kelvin wave appears to decouple from the Rossby wave, which has two positive OLR maxima off the equator in the western Pacific warm pool and subsequently propagates eastward with a much slower speed. Since the low SST in the east Pacific cold tongue region inhibits convection, MJO signals in OLR become weak along the equator, while off-equatorial convection is strengthened to the east of the dateline and across the Panama gap. The MJO propagates into the Caribbean Sea and northwestern subtropical Atlantic as indicated by the significant changes in wind anomalies in these regions. Specifically, in the Caribbean Sea, northeasterly wind anomalies prevailed on May 13 and southwesterly wind anomalies appeared on May 25, as shown in Figure 5a. In the following days, westerly wind anomalies prevail in the western and central tropical Atlantic as the associated convective anomalies move eastward (not shown). This eastward propagation is consistent with the Hovmöller diagram derived from QuikSCAT and OLR anomalies as shown in Figures 2 and 3. The MJO that originates in the Indo-Pacific propagates eastward into the Atlantic, with its maximum

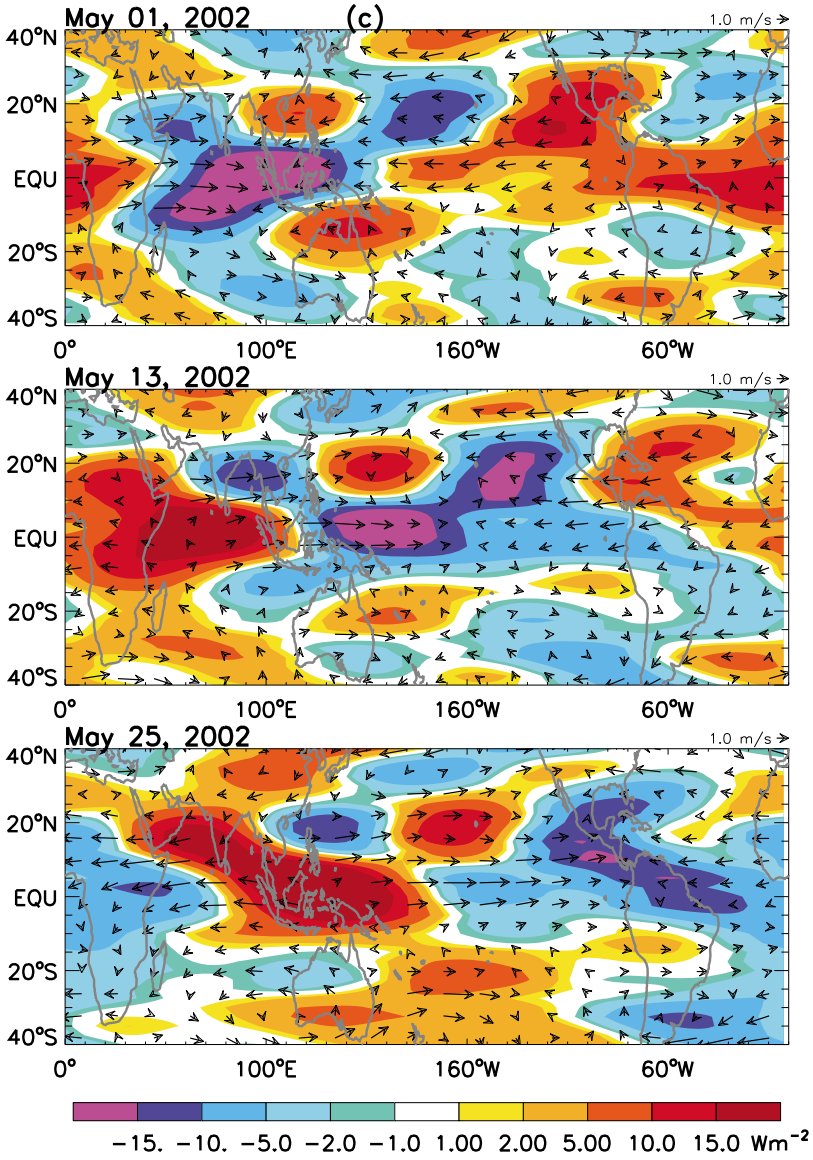

Figure 5. (continued)

influence occurring in the western tropical Atlantic basin, consistent with *Foltz and McPhaden* [2004]. A wider filtering band of 20–100 days and eastward wave numbers 1–6 was also used (figure not shown), and the filtered fields show similar MJO propagation features as in Figure 5c.

[16] The eastward propagation of the off-equatorial convection anomalies is intriguing. These anomalies appear near 160°W, 20°N in the Pacific on May 1 (Figures 5a–5c, top panels). With the eastward propagation of the MJO, the off-equatorial convective anomalies are strengthened and enter the Atlantic via Central America and Isthmus of Panama with a wind anomaly magnitude above 2 m/s (Figures 5a–5c, bottom panels). The Central America and Isthmus of Panama pathway for the MJO surface wind and convection anomalies to enter the Atlantic is consistent among QuikSCAT surface winds, ERA-Interim surface winds, OLR, and precipitation data (Figures 5a–5c). These signals affect the NAM region and generate appreciable convective anomalies in the northwestern subtropical Atlantic Ocean. The eastward propagation during May–June of 30–70 day OLR anomalies averaged from 5°N to 25°N is evident from 160°W to 60°W in a Hovmöoller diagram (Figure 6).

[17] We further analyzed the 2002 period to document variability of OLR and precipitation for the region 5°N–25°N and 180°W–170°W to describe more specifically how off-equatorial convection and related precipitation anomalies in this region are related to the MJO. For example, it is possible that other mechanisms of subseasonal variability such as easterly waves dominate the OLR excursions in this region. In Figure 7, the daily unfiltered OLR time series during 2002 (mean removed) shows that strong convective events that occur in the central Pacific often correspond to negative 30–70 day eastward zonal wave number 1–3 band-pass filtered OLR anomalies (a good proxy for the MJO; *Wheeler and Kiladis* [1999]), which are generally matched

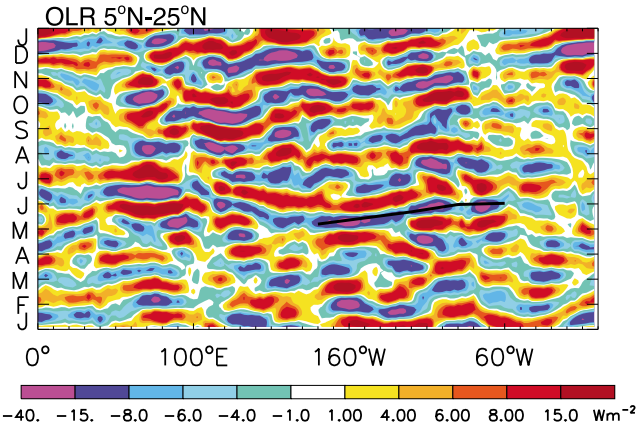

Figure 6. Same as Figure 2a except for 5°N–25°N OLR data.

with the positive 30–70 day precipitation anomalies, indicating that strong convective events shown in daily OLR and the corresponding intraseasonal variations of precipitation are often associated with the MJO.

[18] Detailed analysis of MJO event evolution shows that off-equatorial convective anomalies exist in almost all of the MJO cycles. Why these off-equatorial anomalies propagate eastward with time is an unanswered question, as is the eastward propagation of the MJO in general. Recently, *Pan and Li* [2008] showed that the response pattern of wind and precipitation anomalies in the midlatitudes shifts eastward when tropical heating moves eastward with the MJO. The connection between the off-equatorial convection maxima and OLR anomalies extending northeast and southeast into the midlatitude north and south Atlantic (Figures 5a–5c), respectively, suggests that the gradual eastward shift of midlatitude disturbances [*Higgins and Mo*, 1997] may also interact with this equatorial convection, possibly contributing to its eastward propagation. *Higgins and Mo* [1997] argued that while the MJO can cause midlatitude anomalies through Rossby wave trains, the midlatitude anomalies could feedback onto the tropical precipitation through modification of moisture transport. Eastward propagation in the Intertropical Convergence Zone (ITCZ) could also be affected by interactions between the large-scale MJO flow and tropical synoptic-scale disturbances, through their impacts on the tropospheric moisture budget [e.g., *Maloney*, 2009]. Further investigation of the dynamics that determine the eastward propagation of off-equatorial convection anomalies is beyond the scope of this study, and might be aided by modeling studies.

3.4. Spectral Coherence Analysis During 2002

[19] An analysis of spectral coherence can diagnose the consistency of the phase relationship and amplitude ratio across spectral components in a frequency band for two different time series. Following *Maloney et al.* [2008], we conduct such a spectral coherence analysis here using a reference time series of zonal wind stress averaged over 15°S–15°N and 120°E–160°E, where westerly wind anomalies associated with the MJO achieve large amplitudes [e.g., *McPhaden*, 1999]. Given that observed 40–60 day zonal wind anomalies in the western equatorial Atlantic are most prominent during 2002 from January to July and weaker from August to December (Figure 2; also *Han et al.* [2008, Figure 9a]), we compute the coherence squared and phase in the 30–70 day band between the reference time series and the zonal wind stress at each grid point during January–July 2002 (Figure 8a) separately from August–December 2002 (Figure 8b). A unit vector giving the phase relative to the reference time series is also derived for these periods. The direction of the phase vector indicates the phase relationship between the reference time series and the spatial location of interest. The phase vector of the reference time series is shown in the white area near 140°E, 0°N. A clockwise rotation of the vector indicates increasing phase, and thus the direction of phase propagation.

[20] Coherence squared values exceed 0.5 from the western Pacific to the central Pacific for January–July (Figure 8a), with a phase lag of one-eighth to one-quarter of a cycle relative to the reference point. Although a bit noisy, the general clockwise rotation of the phase vectors indicates eastward progression of zonal wind stress anomalies from the western Pacific to the central Pacific. Near 15°N, zonal wind anomalies propagate from the central Pacific to the Caribbean and tropical north Atlantic basin through Central America and the Isthmus of Panama with coherence squared values of 0.3–0.6, indicating a direct influence of the MJO that propagates from the Pacific into the Atlantic Ocean. In the Atlantic, the coherence squared values exceed 0.5 from the Caribbean Sea to the central equatorial Atlantic basin along the South American coastline with surface wind stress anomalies lagging the reference point by somewhat less than one-quarter of a cycle in the Caribbean Sea to more than one-quarter of a cycle in the equatorial western Atlantic.

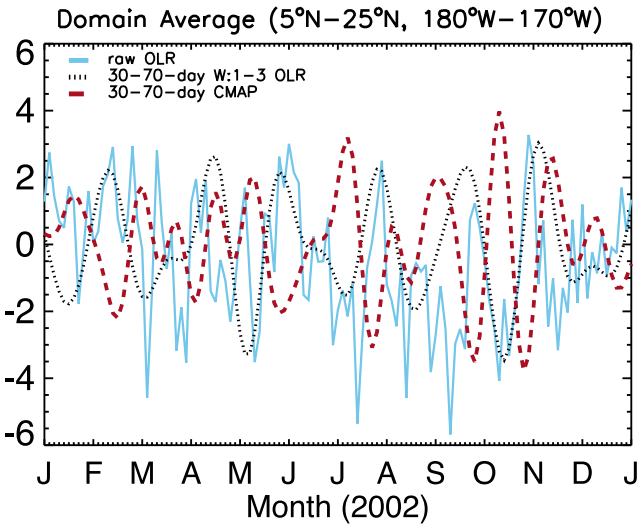

Figure 7. Domain-averaged OLR anomalies (5°N–25°N and 180°W–170°W) during 2002 from raw daily OLR anomaly with the mean removed (blue curve), 30–70 day eastward wave numbers 1–3 filtered OLR (dotted black curve), and 30–70 day filtered CMAP data (dashed red curve). Units for daily OLR anomalies are 8^{-1} w m^{-2}, for filtered OLR anomalies are 3^{-1} w m^{-2}, and for filtered precipitation anomalies are mm day^{-1}.

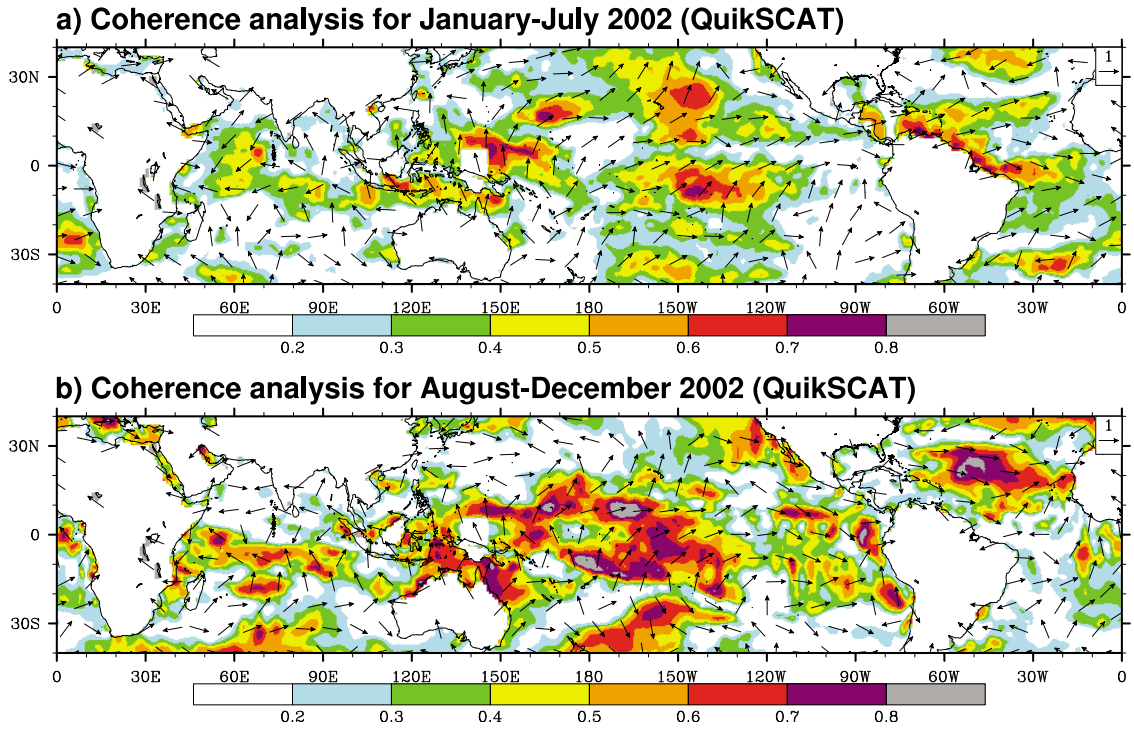

Figure 8. (a) Averaged spectral coherence analysis from January to July 2002 in the 30–70 day band between a reference of surface zonal wind stress (15°S–15°N and 120°E–160°E averaged) and maps of surface zonal wind stress. Filled colors are the coherence squared. Vectors are the phase. The phase vector of the reference is located at the white area at 140°E at the equator. Clockwise rotation indicates phase propagation; (b) same as Figure 8a but for the period from August to December 2002.

The clockwise rotation of the phase vectors suggests MJO propagation along the northeast coastline of the South American continent. One possibility to explore in future work is whether coastal topography in this region acts to propagate wind signals along the northern coast of South America in a similar manner to that of an oceanic Kelvin wave, with the coast to its right in the Northern Hemisphere. The significant surface zonal wind stress anomalies that propagate from the western Atlantic to the central Atlantic along the equator are consistent with the 40–60 day observed surface wind variations from January to July in the work by *Han et al.* [2008]. In the southwest Atlantic, a large area of coherence above 0.3 can also be seen. This is consistent with the analysis of *Jones and Schemm* [2000] demonstrating that the South Atlantic Convergence Zone (SACZ) exhibits a wide range of intraseasonal variability, including 30–70 day variations that are directly related to the MJO.

[21] During August–December 2002 (Figure 8b), large coherence squared values occur in the central Pacific and subtropical Atlantic. The clockwise rotation of the phase vectors and the coherence squared values above 0.4 also show propagation of surface zonal wind anomalies from the western Pacific to Panama. In the equatorial Atlantic, coherence squared values exceeding 0.5 are found in the central and eastern basins but with no obvious eastward propagation. This is consistent with the 40–60 day equatorial surface zonal wind structure during August–December shown by *Han et al.* [2008]. Again, the lack of eastward propagating surface wind signals during summer and fall may reflect the influences of westward propagating Rossby waves and the West African monsoon [e.g., *Grodsky and Carton*, 2001; *Matthews*, 2004; *Maloney and Shaman*, 2008]. Some modest evidence exists for westward propagation along 10°N, as well as some evidence for northward propagation in the eastern Atlantic, consistent with previous studies [e.g. *Maloney and Shaman*, 2008]. Further analysis is needed to confirm the interactions between the westward pathway of the MJO and the West African monsoon.

[22] The above analysis suggests that Atlantic equatorial winds can be strongly influenced by MJO events. Coherence maps for narrow 40–60 day periods (figure not shown) are similar to Figures 8a and 8b, suggesting that the MJO events contribute to the 40–60 day zonal wind variability in the equatorial Atlantic discussed by *Han et al.* [2008]. Figures 9a and 9b show coherence analysis performed using the ERA-Interim 30–70 day surface winds that produce similar results to that from QuikSCAT. The coherence squared values and the clockwise rotation of the phase vectors show the MJO progression during boreal winter and spring of 2002 from the eastern Pacific through Panama and into the western equatorial Atlantic along the South American coastline.

3.5. Statistical Relationships

[23] Above, we focused on intraseasonal variability during 2002, a year when an Atlantic Niño event occurred and strong intraseasonal variability was observed in the

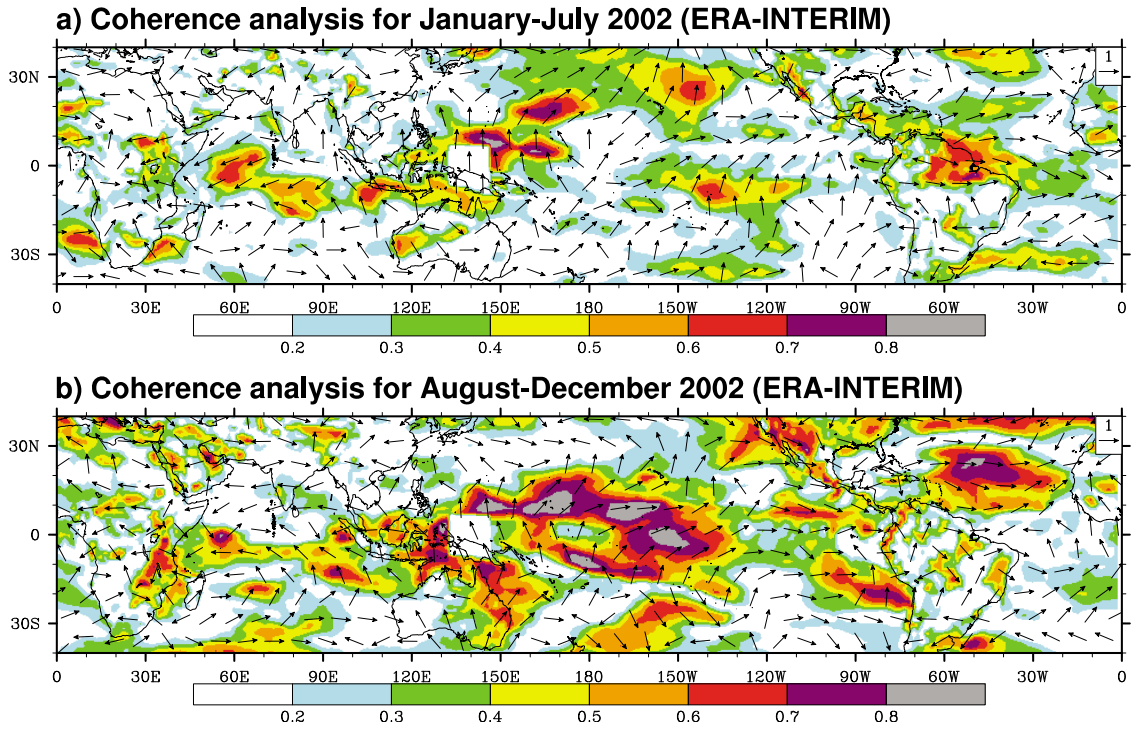

Figure 9. Same as Figure 8 except for 30–70 day ERA-Interim surface zonal wind.

equatorial Atlantic Ocean. Now, we perform coherence analysis for the 30–70 day band during 2000–2006 using QuikSCAT data (Figure 10) and ERA-Interim surface winds (Figure 11). This is done separately for December–May and June–November. We use these periods because the MJO propagation signal and statistics are most robust during these month bands and the nature of the MJO teleconnection to the Atlantic is very different between these

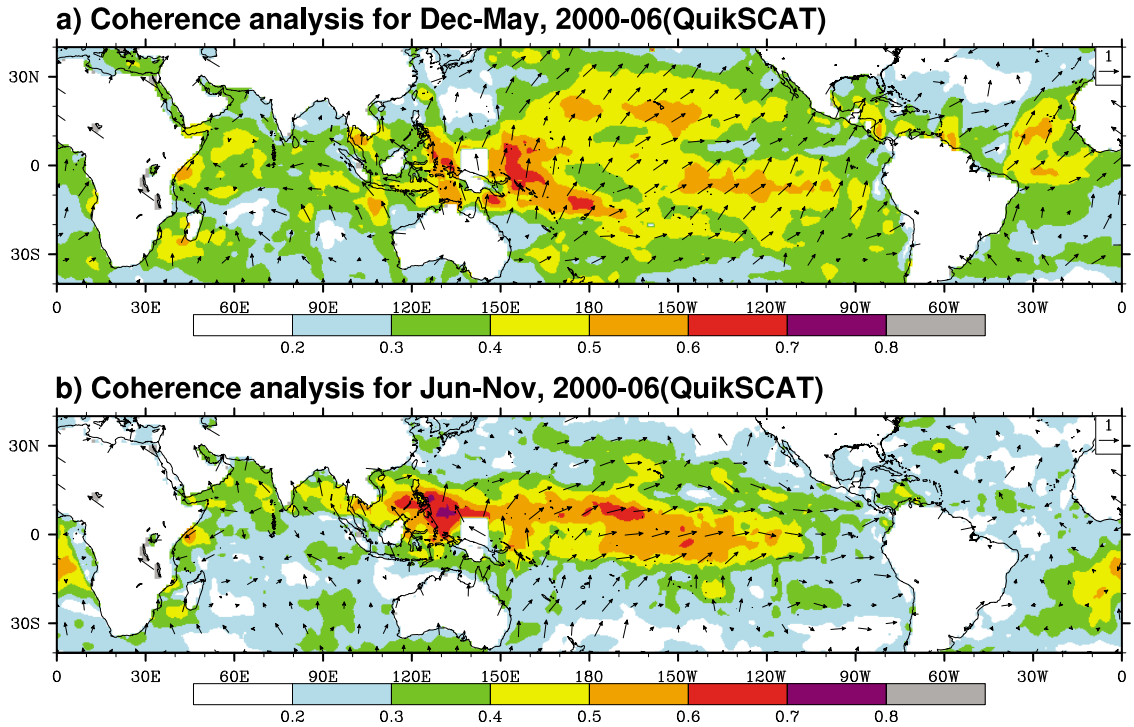

Figure 10. Same as Figure 8 except for longer period averaged 30–70 day QuikSCAT surface zonal wind during December–May and June–November.

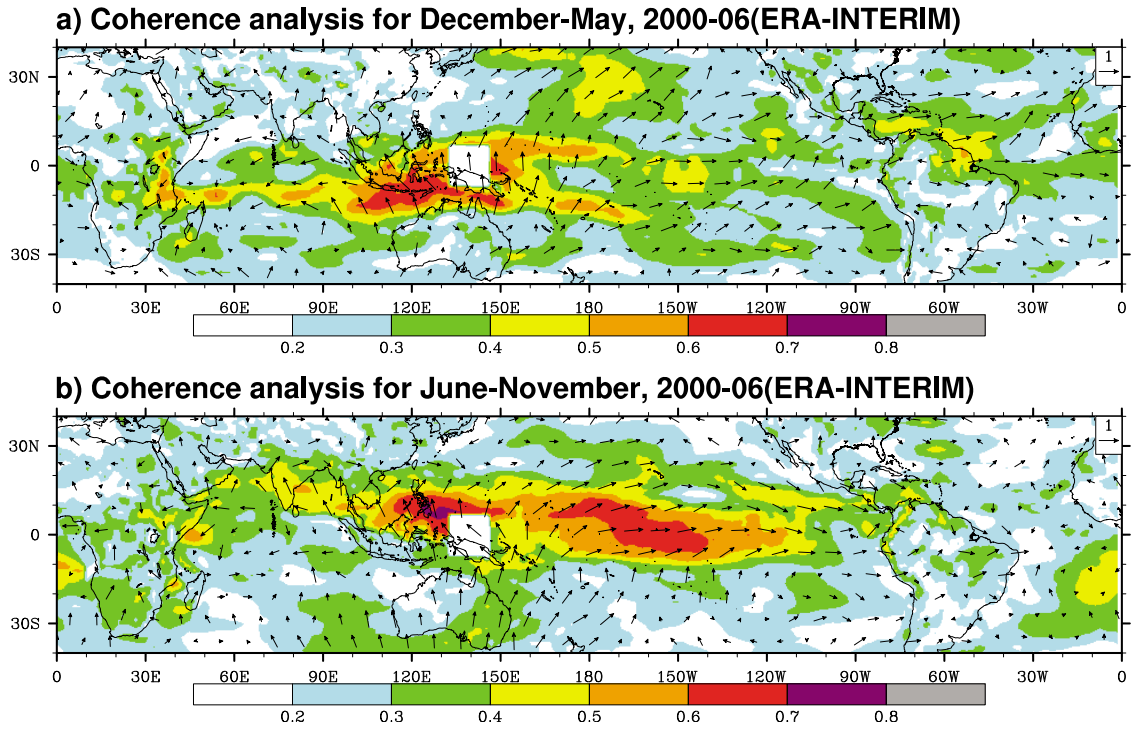

Figure 11. Same as Figure 8 except for longer period averaged 30–70 day ERA-Interim surface zonal wind during December–May and June–November.

two periods (although we did also test different periods, e.g., November–April and May–October). We first obtained the coherence squared for each year in the season of interest, and then averaged these individual coherence estimates over all years. The phase vectors shown in Figures 10 and 11 represent the average of unit phase vectors during individual years across all seven years of the analysis. The amplitude of the phase vector thus represents the consistency of the phase relationship across all years. The eastward propagation of the surface wind anomalies is very obvious from the western Pacific into the eastern Pacific, as indicated by the clockwise rotation of the phase vectors along 15°N during December–May (Figures 10a and 11a), and along 10°N during June–November (Figures 10b and 11b). During December–May (Figures 10a and 11a), the sizeable (>0.4) coherence squared values along the South American coastline to tropical Atlantic Ocean are similar to that of the 2002 case. During June–November, however, the small amplitudes of the phase vectors in Atlantic show the inconsistency of the phase relationship relative to the reference point during 2000–2006, suggesting substantial interannual variability and defined seasonality of the MJO teleconnection to the Atlantic. Note that ERA-Interim data show stronger coherence values than that of QuikSCAT wind in the eastern equatorial Pacific during June–November, but weaker coherences in the central and eastern subtropical Pacific during December–May (compare Figures 10 and 11).

[24] For consistency with the coherence analysis shown in Figures 10 and 11 and to more precisely isolate the seasonal variations of the MJO teleconnection, we calculate the correlation coefficients for December–May and June–November between a reference time series of 30–70 day band-pass filtered zonal wind in the western Pacific (15°S–15°N and 120°E–160°E, averaged) and zonal wind across the tropical oceans, using QuikSCAT surface winds during 2000–2006 and ERA-Interim surface winds during 1990–2007. In Figure 12, correlation maps with the zonal wind index leading by 3, 9, and 15 days, respectively, show a clear eastward progression during December–May and June–November with a maximum correlation coefficient exceeding 0.4 in the eastern Pacific and Panama gap area, and exceeding 0.3 in the Atlantic. These values define the 90% (95%) significance level for QuikSCAT (ERA-Interim) winds. During winter and spring, the MJO significantly affects the equatorial Atlantic and the western subtropical Atlantic Ocean, as indicated by the maximum correlation coefficient of above 0.4 for lags of 9 and 15 days. When the lag is longer than 15 days, the MJO also has a significant influence on the subtropical northern Atlantic during summer and fall with correlation coefficients above 0.3. This delayed influence of MJO on the Atlantic during summer and fall may be due to the strong intraseasonal convective variability in the Western Hemisphere [e.g. *Maloney et al.*, 2008], which makes MJO dynamical signals propagate more slowly due to convective coupling over the east Pacific warm pool. Alternatively, the delayed influence could be due to the different propagation pathways during boreal summer, such as the westward Rossby wave propagation from the Indian Ocean and African monsoon region [*Thorncroft et al.*, 2003; *Sultan and Janicot*, 2003a, 2003b; *Matthews*, 2004]. Correlation maps using ERA40 winds for 1960–2001 were also calculated and produced similar results (figure not shown). Neither the ERA40 nor the ERA-Interim product shows continuous MJO propagation across the South American continent, consistent with the above coherence analysis, and further suggests that the

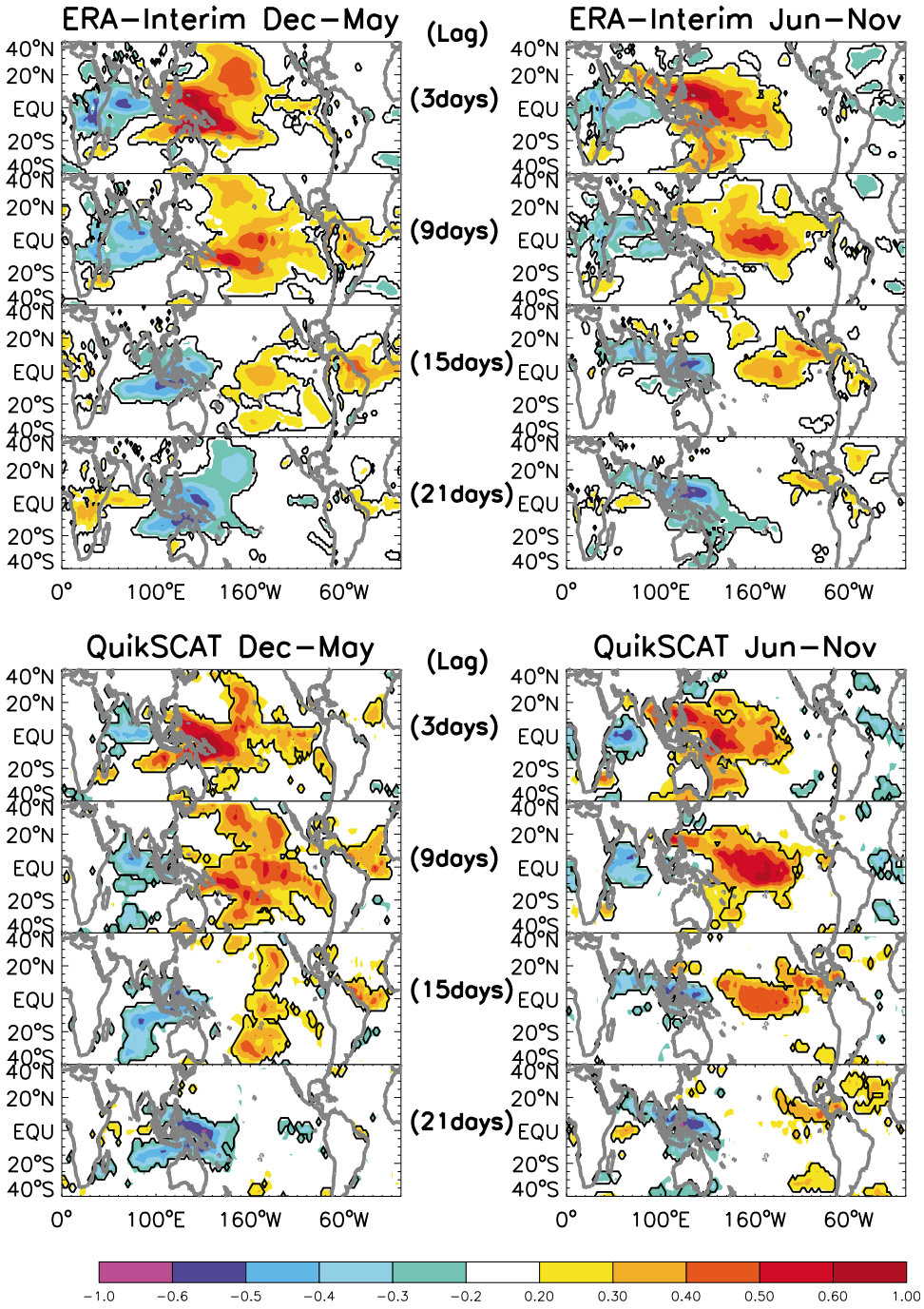

Figure 12. Correlation maps between time series of the 30–70 day zonal wind index of ERA-Interim (1990–2007) and QuikSCAT (2000–2006) in the western Pacific averaged over 15°S–15°N and 120°E–160°E, and zonal wind at each location of 40°S–40°N oceans for lag = 3, 9, 15, and 21 days. December–May (left), and June–November (right). Solid curve shows that the correlation exceeds 90% (95%) significance level for QuikSCAT (ERA-Interim). Note that the significance test takes into account the reduced degrees of freedom due to the filter [*Livezey and Chen*, 1983].

Isthmus of Panama is a critical pathway for the surface signatures of the MJO to propagate into the Atlantic.

4. Summary and Discussion

[25] Eastward propagation of the MJO from the Pacific Ocean to the Atlantic is documented using satellite data and reanalysis products. During 2002, spectral coherence and correlation analysis using QuikSCAT and ERA-Interim winds show that surface signatures of the MJO propagate from the western Pacific into the tropical Atlantic through Central America and the Panama gap, and with further propagation along the northern coastline of South America from the Caribbean Sea to the equatorial Atlantic. MJO

events thus appear to be the primary cause of the observed 40–60 day band-pass filtered zonal surface wind anomalies in the equatorial Atlantic discussed by *Han et al.* [2008].

[26] Strong convection and westerly wind anomalies associated with the MJO first propagate eastward into the western Pacific at a speed of about 5 m/s as a Rossby-Kelvin wave packet. Near the dateline, the Rossby and Kelvin waves decouple, with the Kelvin wave propagating eastward along the equator into the Atlantic at a much faster speed. The off-equatorial convection maxima associated with the Rossby wave also propagates eastward, but at a slower rate. The eastward propagation associated with off-equatorial features is accompanied by the eastward shift of midlatitude convective anomalies, with possible feedbacks onto tropical convection. Another possible mechanism for the eastward propagation of OLR anomalies in the east Pacific ITCZ is the interaction of tropical eddies and the large-scale MJO flow [*Maloney*, 2009]. These possibilities will be explored in future research.

[27] Statistical calculations using QuikSCAT winds for 2000–2006 and ERA-Interim surface data for 1990–2007 show that Atlantic equatorial zonal surface winds are significantly correlated with the intraseasonal zonal winds in the western equatorial Pacific Ocean, a region where westerly wind anomalies associated with the MJO are strong. The maximum correlations exceed 0.4 (significant at the 90% confidence level for QuikSCAT and the 95% confidence level for ERA-Interim) in the equatorial Atlantic region during boreal winter and spring, when the equatorial Atlantic winds lag the western Pacific winds by 9–15 days. The Isthmus of Panama and Central America appear to be an important pathway for the MJO to propagate from the Pacific into the Atlantic, consistent with the spectral coherence analysis during 2002. The MJO impact on Atlantic surface winds during boreal summer and fall is delayed relative to boreal winter and spring, with significant lag correlations apparent after 15 days, which suggests that interactions between the MJO and strong convective variability in the Western Hemisphere may delay MJO impacts. These results are consistent with previous studies showing that the character of the MJO has strong seasonality [*Madden and Julian*, 1994; *Jones et al.*, 2004; *Matthews*, 2000], and were also verified using a long record of ERA40 reanalysis winds for 1960–2001. ERA products show scant evidence of MJO propagation across the South American continent, which further suggests that surface winds associated with the MJO likely propagate into the Caribbean Sea across the Isthmus of Panama and Central America.

[28] Results presented here support the notion that surface wind and convection associated with the MJO can propagate into the Atlantic, affecting the subtropical Atlantic and equatorial regions. The results also suggest pathways for how the MJO can potentially affect the North American monsoon region, in which significant MJO signals have been documented. In 2002, an Atlantic Niño event occurred [*Fu et al.*, 2007], and large amplitude intraseasonal thermocline variability was observed in the equatorial Atlantic [*Han et al.*, 2008]. Our results here show that the strong equatorial intraseasonal zonal wind variations of 2002 result largely from the MJO. One remaining question is whether or not the MJO played a role in triggering the 2002 Atlantic Niño event. This question will be explored in future work.

[29] **Acknowledgments.** Three reviewers provided insightful comments that led to significant improvements in the paper. We thank ECMWF and NCAR for the ERA-40 and ERA-Interim fields. The daily OLR data provided by the NOAA/OAR/ESRL PSD, Boulder, Colorado from their Web site (http://www.cdc.noaa.gov/). The QuikSCAT winds are produced by Remote Sensing Systems and sponsored by the NASA Ocean Vector Winds Science Team (OVWST). Weiqing Han is supported by NASA Ocean Vector Wind Science Team award 1283568 and NSF CAREER award OCE 0847605. The National Center for Atmospheric Research is supported by NSF. EDM was supported by NSF Climate and Large-Scale Dynamics Grant Numbers 0946911 and 0828531. EDM was also supported under Award# NA08OAR4320893 from NOAA. The statements, findings, conclusions, and recommendations do not necessarily reflect the views of NSF, NOAA, or the Department of Commerce.

References

Allan, R. P., B. J. Soden, V. O. John, W. Ingram, and P. Good (2010), Current changes in tropical precipitation, *Environ. Res. Lett.*, *5*, 025205, doi:10.1088/1748-9326/5/2/025205.

Arkin, P. A., and P. E. Ardanuy (1989), Estimating climatic-scale precipitation from space: A review, *J. Clim.*, *2*, 1229–1238.

Barlow, M., and D. Salstein (2006), Summertime influence of the Madden-Julian oscillation on daily rainfall over Mexico and Central America, *Geophys. Res. Lett.*, *33*, L21708, doi:10.1029/2006GL027738.

CLIVAR Madden-Julian Oscillation (MJO) Working Group (2009), MJO simulation diagnostics, *J. Clim.*, *22*, 3006–3030, doi:10.1175/2008JCLI2731.1.

Duchon, C. E. (1979), Lanczos filtering in one and two dimensions, *J. Appl. Sci.*, *61*, 1004–1023.

Foltz, G. R., and M. J. McPhaden (2004), The 30–70 day oscillations in the tropical Atlantic, *Geophys. Res. Lett.*, *31*, L15205, doi:10.1029/2004GL020023.

Fu, R., M. Young, H. Wang, and W. Han (2007), Investigate the influence of the Amazon rainfall on westerly wind anomalies and the 2002 Atlantic Niño using QuikScat, Altimeter, and TRMM data, presented at joint NASA OVWST 2007 Meeting, 2007 EUMETSAT Meteorological Satellite Conference, and 15th Satellite Meteorological and Oceanography Conference, Am. Meteorol. Soc., Amsterdam, Neth.

Grodsky, S. A., and J. A. Carton (2001), Coupled land/atmosphere interactions in the West African Monsoon, *Geophys. Res. Lett.*, *28*, 1503–1506, doi:10.1029/2000GL012601.

Han, W., P. J. Webster, J.-L. Lin, W. T. Liu, R. Fu, D. Yuan, and A. Hu (2008), Dynamics of intraseasonal sea level and thermocline variability in the equatorial Atlantic during 2002–2003, *J. Phys. Oceanogr.*, *38*, 945–967.

Han, W., T. Shinoda, L. Fu, and J. P. McCreary (2006), Impact of atmospheric intraseasonal oscillations on the Indian Ocean Dipole during the 1990s, *J. Phys. Oceanogr.*, *36*, 670–690.

Hendon, H. H., and M. L. Salby (1994), The life cycle of the Madden-Julian oscillation, *J. Atmos. Sci.*, *51*, 2225–2237, doi:10.1175/1520-0469(1994)051<2225:TLCOTM>2.0.CO;2.

Higgins, R. W., and K. C. Mo (1997), Persistent North Pacific circulation anomalies and the tropical intraseasonal oscillation, *J. Clim.*, *10*, 3028–3046.

Higgins, R. W., and W. Shi (2001), Intercomparison of the principal modes of interannual and intraseasonal variability of the North American monsoon system, *J. Clim.*, *14*, 403–417.

Janicot, S., F. Mounier, N. M. J. Hall, S. Leroux, B. Sultan, and G. N. Kiladis (2009), Dynamics of the west African monsoon, Part IV: Analysis of 25–90 day variability of convection and the role of the Indian monsoon, *J. Clim.*, *22*, 1541–1565.

Jones, C., and J. E. Schemm (2000), The influence of intraseasonal variations on medium to extended range weather forecasts over South America, *Mon. Weather Rev.*, *128*, 486–494.

Jones, C., and M. V. Carvalho (2006), Changes in the activity of the Madden-Julian Oscillation during 1958–2004, *J. Clim.*, *19*, 6353–6370.

Jones, C., M. V. Carvalho, R. W. Higgins, D. E. Waliser, and J. K. E. Schemm (2004), Climatology of tropical intraseasonal convective anomalies: 1979–2002, *J. Clim.*, *17*, 523–539.

Kessler, W. S., and R. Kleeman (2000), Rectification of the Madden-Julian oscillation into the ENSO cycle, *J. Clim.*, *13*, 3560–3575.

Krishnamurti, T. N., and D. Subramanyam (1982), The 30–50 day mode at 850 mb during MONEX, *J. Atmos. Sci.*, *39*, 2088–2095.

Lau, K. M., and D. E. Waliser (Eds) (2005), *Intraseasonal Variability in the Atmosphere-Ocean Climate System*, Praxis Publ., Chichester, U. K.

Lawrence, D. M., and P. J. Webster (2001), Interannual variations of the intraseasonal oscillation in the south Asian summer monsoon region, *J. Clim.*, *14*, 2910–2922.

Liebmann, B., and C. A. Smith (1996), Description of a complete (interpolated), outgoing longwave radiation dataset, *Bull. Am. Meteorol. Soc.*, *77*, 1275–1277.

Livezey, R. E., and W. Y. Chen (1983), Statistical field significance and its determination by Monte Carlo Techniques, *Mon. Weather Rev.*, *111*, 46–59.

Lorenz, D. J., and D. L. Hartmann (2006), The effect of the MJO on the North American monsoon, *J. Clim.*, *19*, 333–343, doi:10.1175/JCLI3684.1.

Madden, R. A., and P. R. Julian (1971), Detection of a 40–50 day oscillation in the zonal wind in the tropical Pacific, *J. Atmos. Sci.*, *28*, 702–708.

Madden, R. A., and P. R. Julian (1994), Observations of the 40–50 day tropical oscillation: A review, *Mon. Weather Rev.*, *122*, 814–837.

Maloney, E. D. (2009), The moist static energy budget of a composite tropical intraseasonal oscillation in a climate model, *J. Clim.*, *22*, 711–729.

Maloney, E. D., and D. L. Hartmann (2000), Modulation of eastern North Pacific hurricanes by the Madden-Julian oscillation, *J. Clim.*, *13*, 1451–1460.

Maloney, E. D., and J. Shaman (2008), Intraseasonal variability of the West African monsoon and Atlantic ITCZ, *J. Clim.*, *21*, 2898–2918.

Maloney, E. D., D. B. Chelton, and S. K. Esbensen (2008), Subseasonal SST variability in the tropical eastern North Pacific during boreal summer, *J. Clim.*, *21*, 4149–4167.

Martin, E. (2010), Caribbean precipitation and the MJO, presented at 29th Conference on Hurricanes and Tropical Meteorology, Am. Meteorol. Soc., Tucson, AZ.

Matthews, A. J. (2000), Propagation mechanisms for the Madden-Julian Oscillation, *Q. J. R. Meteorol. Soc.*, *126*, 2637–2651.

Matthews, A. J. (2004), Intraseasonal variability over tropical Africa during northern summer, *J. Clim.*, *17*, 2427–2440.

McPhaden, M. J. (1999), Genesis and evolution of the 1997–98 El Niño, *Science*, *283*, 950–954, doi:10.1126/science.283.5404.950.

Moore, A. M., and R. Kleeman (1999), Stochastic forcing of ENSO by the intraseasonal oscillation, *J. Clim.*, *12*, 1199–1200.

Pan, L. L., and T. Li (2008), Interactions between the tropical ISO and midlatitude low-frequency flow, *Clim. Dyn.*, *31*, 375–388.

Rao, S. A., and T. Yamagata (2004), Abrupt termination of Indian Ocean Dipole events in response to intraseasonal oscillations, *Geophys. Res. Lett.*, *31*, L19306, doi:10.1029/2004GL020842.

Salby, M. L., and H. H. Hendon (1994), Intraseasonal behavior of clouds, temperature, and motion in the tropics, *J. Atmos. Sci.*, *51*, 2207–2224.

Sikka, D. R., and S. Gadgil (1980), On the maximum cloud zone and the ITCZ over Indian longitudes during southwest monsoon, *Mon. Weather Rev.*, *108*, 1840–1853.

Simmons, A., S. Uppala, D. Dee, and S. Kobayashi (2007), ERA-Interim: New ECMWF reanalysis products from 1989 onwards, *ECMWF Newsl.*, *110*, 25–35.

Small, R. J., S.-P. Xie, E. D. Maloney, S. P. de Szoeke, and T. Miyama (2010), Intraseasonal Variability in the far-east Pacific: Investigation of the role of air-sea coupling in a regional coupled model, *Clim. Dyn.*, *34*, 1–24, doi:10.1007/s00382-010-0786-2.

Sultan, B., and S. Janicot (2003a), The West African monsoon dynamics: Part I, documentation of intraseasonal variability, *J. Clim.*, *16*, 3389–3406.

Sultan, B., and S. Janicot (2003b), The West African monsoon dynamics: Part II, the "preonset" and "onset" of the summer monsoon, *J. Clim.*, *16*, 3407–3427.

Takayabu, Y. N., T. Iguchi, M. Kachi, A. Shibata, and H. Kanzawa (1999), Abrupt termination of the 1997–98 El Niño in response to a Madden-Julian oscillation, *Nature*, *402*, 279–282, doi:10.1038/46254.

Thorncroft, C. D., et al. (2003), The JET2000 project, aircraft observations of the African easterly jet and African easterly waves, *Bull. Am. Meteorol. Soc.*, *79*, 815–829.

Wang, B., and X. Xie (1997), A model for the boreal summer intraseasonal oscillation, *J. Atmos. Sci.*, *54*, 72–86.

Webster, P. J. (1983), Mechanisms of monsoon transition: Surface hydrology effects, *J. Atmos. Sci.*, *40*, 2110–2124.

Wheeler, M., and G. N. Kiladis (1999), Convectively coupled equatorial waves: Analysis of clouds and temperature in the wave number–frequency domain, *J. Atmos. Sci.*, *56*, 374–399.

Wheeler, M. C., and H. H. Hendon (2004), An all season real time multivariate MJO index: Development of an index for monitoring and prediction, *Mon. Weather Rev.*, *132*, 1917–1932.

Xie, P., and P. A. Arkin (1997), Global precipitation: A 17 year monthly analysis based on gauge observations, satellite estimates, and numerical model outputs, *Bull. Am. Meteorol. Soc.*, *78*, 2539–2558.

Yasunari, T. (1981), Structure of an Indian summer monsoon system with around 40 day period, *J. Meteorol. Soc. Jpn.*, *59*, 336–354.

D. Gochis and W. Yu, Research Applications Laboratory, National Center for Atmospheric Research, P.O. Box 3000, Boulder, CO 80307-3000, USA. (weiyu@ucar.edu)

W. Han, Department of Atmospheric and Oceanic Sciences, University of Colorado, Boulder, CO 80309-0311, USA.

E. D. Maloney, Department of Atmospheric Science, Colorado State University, 1371 Campus Delivery, Fort Collins, CO 80523-1371, USA.

S.-P. Xie, International Pacific Research Center, University of Hawaii, 1680 East-West Rd., Honolulu, HI 96822, USA.